Contents lists available at ScienceDirect

Archives of Biochemistry and Biophysics

Characterization of hydroxymethylpyrimidine phosphate kinase from mesophilic and thermophilic bacteria and structural insights into their differential thermal stability

Pablo A. Cea[a], Gissela Araya[a], Gabriel Vallejos[a], Rodrigo Recabarren[b], Jans Alzate-Morales[b], Jorge Babul[a], Victoria Guixé[a], Victor Castro-Fernandez[a,*]

[a] Departamento de Biología, Facultad de Ciencias, Universidad de Chile, Santiago, Chile
[b] Centro de Bioinformática, Simulación y Modelado, Facultad de Ingeniería, Universidad de Talca, Talca, Chile

ARTICLE INFO

ABSTRACT

The hydroxymethylpyrimidine phosphate kinases (HMPPK) encoded by the thiD gene are involved in the thiamine biosynthesis pathway, can perform two consecutive phosphorylations of 4-amino-5-hydroxymethyl-2-methyl pyrimidine (HMP) and are found in thermophilic and mesophilic bacteria, but only a few characterizations of mesophilic enzymes are available. The presence of another homolog enzyme (pyridoxal kinase) that can only catalyze the first phosphorylation of HMP and encoded by pdxK gene, has hampered a precise annotation in this enzyme family. Here we report the kinetic characterization of two HMPPK with structure available, the mesophilic and thermophilic enzyme from Salmonella typhimurium (StHMPPK) and Thermus thermophilus (TtHMPPK), respectively. Also, given their high structural similarity, we have analyzed the structural determinants of protein thermal stability in these enzymes by molecular dynamics simulation. The results show that pyridoxal kinases (PLK) from gram-positive bacteria (PLK/HMPPK-like enzymes) constitute a phylogenetically separate group from the canonical PLK, but closely related to the HMPPK, so the PLK/HMPPK-like and canonical PLK, both encoded by pdxK genes, are different and must be annotated distinctly. The kinetic characterization of StHMPPK and TtHMPPK, shows that they perform double phosphorylation on HMP, both enzymes are specific for HMP, not using pyridoxal-like molecules as substrates and their kinetic mechanism involves the formation of a ternary complex. Molecular dynamics simulation shows that StHMPPK and TtHMPPK have striking differences in their conformational flexibility, which can be correlated with the hydrophobic packing and electrostatic interaction network given mainly by salt bridge bonds, but interestingly not by the number of hydrogen bond interactions as reported for other thermophilic enzymes.

Enzymes: EC 2.7.1.49, EC 2.7.4.7, EC 2.7.1.35, EC 2.7.1.50

1. Introduction

Thiamin pyrophosphate, the active form of vitamin B1, is an essential cofactor in all living systems and is synthesized through phosphorylation of thiamin phosphate. The precursors for thiamin phosphate are HMP-PP (4-amino-5-hydroxymethyl-2-methylpyrimidine pyrophosphate) and THZ-P (4-methyl-5-β-hydroxyethylthiazole phosphate), which are formed in separated metabolic branches and then coupled together by thiamin phosphate synthase. In bacteria like Escherichia coli, the HMP and thiazole moiety can be synthesized de novo or salvaged for reuse in thiamin synthesis [1]. The crucial salvage step of the thiazole moiety is the ATP-dependent phosphorylation to THZ-P by the THZ kinase (EC 2.7.1.50), while salvage of HMP is accomplished by its phosphorylation to HMP-P, by the HMP kinase activity (HMPK, EC 2.7.1.49). Interestingly, the enzyme with this activity is able to catalyze two related reactions in consecutive steps; besides the
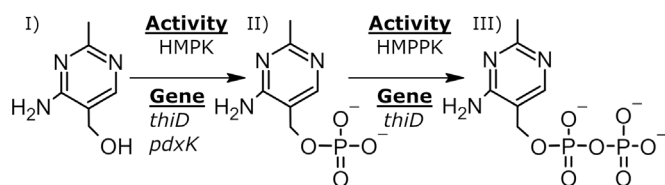
Fig. 1. Synthesis of HMP-PP in the thiamine biosynthesis pathway.
I. HMP, II. HMP-P, III. HMP-PP. The first step in the path corresponds to the phosphorylation of HMP (HMPK activity), which can be made by the products of the *thiD* and *pdxK genes*. The second step is the incorporation of a second phosphate (HMPPK activity), which can only be made by the enzyme coded by the *thiD* gene.

phosphorylation of HMP to give HMP-P, the same enzyme catalyzes the phosphorylation of its reaction product to generate hydroxymethylpyrimidine pyrophosphate (HMPPK, EC 2.7.4.7) being this last reaction an essential step for the biosynthesis of thiamin pyrophosphate [2]. In both reactions, the phosphoryl donor is ATP and the gene that encodes for this enzyme is denominated *thiD* (Fig. 1), which was first described in *Escherichia coli* [3].

Nonetheless, HMP can also be phosphorylated by pyridoxal kinase (PLK, EC 2.7.1.35) an enzyme that participates in the synthesis of pyridoxal phosphate (vitamin B6) [4,5], encoded by the *pdx*K gene.

Structure determination has allowed to classify these three kinases (HMPPK, THZ, and PLK) as homologs and members of the vitamin kinases family that belongs to the ribokinase superfamily [6]. Members of this superfamily accept a wide range of substrates, all of which are phosphorylated at a hydroxyl group. Surprisingly, the HMPPK enzyme, as mentioned above, catalyzes another type of phosphorylation, where the phosphate group is transferred to a phosphomethyl group of HMP-P. To date, HMPPK enzymes from *E. coli*, *B. subtilis*, and *S. aureus* have been experimentally proven to perform two consecutive phosphorylation steps [5,7,8]. Unfortunately, no crystallographic structures are available for these enzymes. Nevertheless, uncharacterized *in vitro* HMPK from *S. typhimurium* and *T. thermophilus* are deposited on the protein data bank (PDB: 1JXH and 1UB0, respectively). Differently, the structures of several PLK have been determined and their enzymatic properties were characterized [9–12]. Although PLK and HMPPK enzymes are homologs and have similar active sites, they display very different catalytic properties. Beside HMP, pyridoxal kinase can catalyze the mono-phosphorylation of pyridoxal, pyridoxine, and pyridoxamine to their 5′ phosphates, while HMPPK has been reported to only participate in the thiamine synthesis pathway, being able only to phosphorylate HMP and HMP-P.

The presence of two different enzymes able to catalyze the phosphorylation of HMP (PLK and HMPPK) encoded by different homologs genes (*pdxK* and *thiD*), has generated miss annotation of gene functions in this family. Initially, the gene responsible for the phosphorylation of HMP to HMP-P in *E. coli* was named *thiJ* and later, it was demonstrated that its product was the same as that of the *pdxK* gene (PLK enzyme) and that the product of the *thiD* gene, beside HMPPK activity, also exhibited HMP kinase activity [8,13]. In *Bacillus subtilis,* the gene product initially annotated as *thiD* had HMP kinase and PLK activity and therefore it was re-annotated as *pdx*K, whereas the gene initially identified as *yjbV* was later re-annotated as *thiD*, since it has HMPK and HMPPK activity [5]. A similar misunderstanding occurred with the HMP kinase activity present in *S. aureus*, where the PLK was misannotated as HMPPK (phosphomethylpyrimidine kinase, UniProt A0A0H3JTP0), but was demonstrated that have PLK and HMPK activity [11,14].

Structural analysis of the active site of bacterial enzymes annotated as PLK revealed two distinct groups; the first one being highly similar to eukaryotic pyridoxal kinases, whereas the second is similar to HMPPKs and have been only reported in Gram positive bacteria. This led Newman et al. [10] to propose this group of enzymes as a new subclass

called "PLK/HMPP kinase-like". Likewise, Nodwell et al. described that PLK (PLK/HMPPK-like) from *S. aureus* is a new sub-family of enzymes, different from those encoded by the canonical *pdxK* gene [11]. Analysis of the evolutive history of the bifunctional HMPK-PLK activity trait of PLK/HMPPK-like, employing ancestral enzyme reconstruction, showed that the common ancestor between HMPPK and PLK/HMPPK-like was specific for HMP, showing that the emergence of PLK activity in the PLK/HMPPK-like group corresponds to a parallel event with respect to the canonical PLKs, as it was previously hypothesized [10,15]. However, a complete picture of the phylogenetic relationships between PLK, HMPPK and PLK/HMPPK-like enzymes is missing. For this purpose, we performed a phylogenetic analysis and the results obtained contribute to shed light on the gene annotation of PLK/HMPPK-like and canonical PLK enzymes.

Structurally, the only crystallographic structures available for HMPPK enzymes are the ones from *Salmonella typhimurium (StHMPPK)* and *Thermus termophillus (TtMPPK)*. Although these enzymes only share 52% of sequence identity, they have an almost identical structure with an RMSD of 1.2 Å. Moreover, they belong to bacterial species that inhabit ecological niches with very different temperatures and no biochemical or kinetic information is available for them. To asses if the double phosphorylation and substrate specificity traits described for HMPPK are ubiquitous and conserved, we performed the kinetic characterization of both enzymes. Furthermore, we also carried out computational studies to explore the structural differences responsible for their differential thermal stability, showing that these proteins constitute an excellent model to study differences in this property given their homology and high structural similarity.

2. Materials and methods

2.1. Multiple sequence alignment and phylogenetic inference

Sequences were retrieved by a direct search of proteins annotated as ThiD, PdxK, and PdxY from the UniProtKB database [16]. A multiple sequence alignment with structural restrictions was built with Promals3D [17], using the structural information derived from the crystallographic structures of the HMPPK from *S. typhimurium* (PDB 1JXI) and *T. thermophilus* (PDB 1UB0), and the PLK/HMPPK-like from *S. aureus* (PDB 4C5J) and *B. subtilis* (PDB 2I5B). The evolutionary model was chosen using ProtTest v3.4.2. through AICc and Bayes Information Criterion (BIC) [18]. A maximum-likelihood phylogenetic tree was built employing PhyML, using an LG matrix as fixed model, with gamma-shaped variation across sites and a proportion of invariant sites [19]. Node robustness was assessed by the likelihood ratio test.

2.2. Protein expression and purification

The genes for *StHMPPK* (UniProt P55882) and *TtHMPPK* (UniProt Q5SKG3) were synthesized (Genscript, Piscataway, NJ, USA) with N-terminal His tag, TEV cleavage site, codon-optimized for expression in *E. coli*, cloned in the modified pET-TEV-15b vector and expressed in *E. coli* BL21(DE3). Cells were cultured at 37 °C, containing 100 μg/mL ampicillin in LB and terrific broth for *StHMPPK* and *TtHMPPK*, respectively. Protein expression was induced by adding 0.5 mM isopropyl-ᴅ-thiogalactopyranoside at OD600 0.5–0.6 and 0.8 for *StHMPPK* and *TtHMPPK*, respectively. The cultures were grown overnight at 30 °C and the cells were harvested by centrifugation, re-suspended in binding buffer (50 mM Tris HCl pH 7.8, 500 mM NaCl and 20 mM imidazole) with 1 mM PMSF (phenylmethylsulfonyl fluoride) and disrupted by sonication. After centrifugation ($18.514 \times g$ for 20 min at 4 °C), *TtHMPPK* was heated at 70 °C for 10 min, chilled on ice, and centrifuged again. The soluble fractions were loaded onto a Ni^{+2}-Sepharose affinity column (HisTrap HP, GE Healthcare). The proteins were eluted with a linear gradient of imidazole between 20 and 500 mM and fractions containing enzyme activity were pooled. After

the affinity chromatography, *StHMPPK* was dialyzed against 50 mM Tris-HCl pH 8.4, 100 mM arginine and 20% glycerol. *TtHMPPK* was dialyzed against 50 mM Tris-HCl pH 8, 300 mM NaCl, 100 mM arginine and 20% glycerol. Protein concentration was determined using the Bio-Rad protein assay (Bio-Rad, Hercules, CA, USA) and BSA Standard (Bovine serum albumin, Thermo Fisher Scientific Inc., Waltham, MA, USA) as a reference. Enzymes purity was analyzed by SDS-PAGE stained with Coomassie Blue and purified proteins were stored at −80 °C in presence of 20% glycerol.

2.3. Anion exchange by HPLC

The appearance of HMP, HMP-P, and HMP-PP during the reaction time was analyzed by high performance liquid chromatography (Waters 1525 HPLC) using an anion exchange column (MonoQ HR 5/5, Pharmacia Biotechnology), in 25 mM Tris-HCl pH 7.5 and a gradient from 0 to 35% of 1 M NaCl at 1 mL/min. The phosphorylated products were measured by absorbance at 235 nm (Waters 2487 absorbance detector). The enzymatic reaction was stopped at different incubation times with 50 mM EDTA and the protein was removed from the sample by ultrafiltration (10 kDa cutoff Amicon, Sigma-Aldrich). 20 μL samples were loaded in the column.

2.4. Kinase activity assay

HMPK activity was measured following the appearance of ADP in a coupled assay with pyruvate kinase/lactate dehydrogenase, measuring the oxidation of NADH at 340 nm in a photodiode array spectrophotometer (Hewlett Packard/Agilent 8453). The coupled assay contained 0.8 U/mL of pyruvate kinase and 2.4 U/mL of lactate dehydrogenase, both from rabbit muscle (Sigma-Aldrich), 0.3 mM phosphoenolpyruvate (PEP), 125 mM KCl and 0.2 mM NADH. Enzyme units (U) were calculated using an extinction coefficient of 6.22 mM^{-1} cm^{-1} for NADH and defined as μmoles/min of ADP. Substrate specificity and ADP titration assays were performed in 50 mM HEPES pH 7.0.

2.5. Steady-state models of enzyme kinetics

The HMP apparent K_m and V_{max} kinetic parameters for *STHMPPK* and *TtHMPPK* were determined using a UV/visible Synergy 2 spectrophotometer (BioTek, Winooski, VT, USA) and 96-well plates (model 269620; Nunc, Rochester, NY, USA); the measurements were performed at 25 °C with 25 mM HEPES pH 8.0, an extinction coefficient of 6.22 $mM^{-1}cm^{-1}$ for NADH and a path length correction at 1 cm was used for specific activity (U/mg, U = μmol/min) determinations. For both enzymes the HMP saturation curves were obtained measuring initial rates (v_0) varying the HMP concentration at constant MgATP concentrations. All curves were adjusted to the data using a Michaelian (hyperbolic) (Equation (1)) and a Hill model (Equation (2)). Akaike's informative criteria (AICc) was used to discriminate between models. Considering the kinetic mechanism described for ribokinase superfamily members [20], we used a sequential ordered mechanism to obtain the true K_M for HMP and MgATP from Fig. 4B using equation (3). This equation describes a hyperbolic function that intersects the Y-axis at a non-zero value, which intersects corresponds to α/β. In the case where HMP is the first substrate (A), α is equal to $K_{ia}K_b$ and β is defined as K_b. Otherwise, if HMP is the second substrate (B) to bind to the enzyme, α is equal to $K_{ia}K_b/K_a$ and β corresponds to K_a [21]. It should be noted that in both cases, β represents the K_M for MgATP.

$$v_0 = \frac{V_{max}[S]}{K_M + [S]}$$

                                                          Equation 1

$$v_0 = \frac{V_{max}[S]^h}{K' + [S]^h}$$

                                                          Equation 2

$$K_M{}^{app}HMP = \frac{\alpha + K_M{}^{HMP}[ATP]}{\beta + [ATP]}$$

                                                          Equation 3

2.6. Thermal stability

Protein thermal stability of *StHMPPK* and *TtHMPPK* was analyzed monitoring the loss of secondary structure content in a Jasco spectropolarimeter (J-1500), coupled to a Peltier temperature control system (PTC-517) following the molar ellipticity at 222 nm and using a 1 mm path length cuvette. The protein concentration for both proteins was 0.2 mg/mL in 50 mM sodium phosphate buffer pH 7.8. Due to irreversible denaturation, the change in CD signal was monitored with a change in temperature of 0.5, 1.0, 2.0 and 3 °C/min. Native state spectra were acquired at 25 °C using a scanning speed of 50 nm/min, using the same buffer and protein concentration. Each spectrum is the average of three accumulated (scans).

2.7. All-atom explicit solvent molecular dynamics simulation of StHMPPK and TtHMPPK

Crystal structures of *StHMPPK* and *TtHMPPK* (PDB: 1JXH and 1UB0, respectively), were used as initial coordinates to build the molecular systems. Missing loops were added using Modeller v9.15. The protonation states were assigned using the Propka software [22] implemented in Maestro visualization software (Maestro (2014) *Version 9.7*, Schrödinger, LLC, New York, NY). The structures were solvated in a TIP3P water orthorhombic box [23] with a 10 Å extension over the protein surface using *tleap* from Ambertools14 [24]. Counter-ions (Na^+ and Cl^-) were placed as needed within the boxes to maintain the electroneutrality of each system. All calculations were performed using the parameters derived from the *ff99SB* force field [25]. Energy minimizations were carried out following six successive stages of minimization, wherein each minimization cycle consisted in 1,000 steps using the steepest descent algorithm followed by 1,000 steps using a conjugated gradient method. In the first stage, a harmonic positional restraint of 500 kcal/mol Å^2 was applied over the heavy solute atoms to accommodate the solvent and the hydrogens of the protein. In the following five stages, minimizations were carried out successively reducing the restraint from 50 to 5 kcal/mol Å^2. The minimized systems were equilibrated under NVT conditions, heating the system from 100 K to 300 K using the weak-coupling Berendsen thermostat [26,27] in a window of 200 ps. Then, 10 ns-long equilibrations in NPT conditions were carried out for each system, keeping a constant temperature of 300 K using the Berendsen thermostat and constant pressure of 1 atm using the Berendsen barostat. Finally, two independent production MDS of 40 ns were performed for each system under the same conditions of the NPT equilibration with no restraints. All the simulations were done using the Amber14 software [28], using periodic boundary conditions with a time step of 2 fs. The SHAKE algorithm [29] for bond lengths constraints involving hydrogen atoms was used. Non-bonded interactions were calculated using a cut-off of 8 Å and the Particle Mesh Ewald method [30] was used for treating long-range electrostatic interactions.

The RMSD of the systems was calculated using the RMSD trajectory tool in VMD. For RMSF calculations, a reference structure was obtained by choosing a representative frame using the cluster function available in *cpptraj* [31]. For this, the structures produced during the MDS trajectories were clustered using the density-based scan algorithm with an epsilon value of 1.0 Å for Cα RMSD and 25 minimum points. The RMSF was calculated aligning the structures in the trajectories to the representative structure using *cpptraj*.

Salt bridge (SB) interactions were determined using the Salt-Bridge plugin for VMD [32]. The interactions were defined using a cut-off distance of 4.5 Å between the oxygen-nitrogen pair. Interactions lasting less than 10% of the simulation time were discarded.

To determine the amino acid composition in the core of each

protein, the molecular surface per residue was calculated using the WHAT-IF web server [33] employing the representative structure chosen as described earlier. Residues with a molecular surface < 5 Å² were considered to be part of the core, otherwise they were considered to be exposed. The interatomic hydrophobic interactions were quantified using the native contacts function implemented in *cpptraj*. The native contacts between hydrophobic residues in each simulation frame were identified using a cut-off distance of 5 Å and ignoring hydrogen atoms and interactions between residues spaced less than three positions apart within the peptide sequence.

3. Results

3.1. Phylogenetic tree of enzymes with HMP kinase activity

To determine the phylogenetic relationships among the bacterial enzymes that display HMP kinase activity, we constructed a multiple sequence alignment to build a maximum likelihood phylogenetical tree. For this purpose, we retrieved sequences annotated as ThiD (HMPPK products of *thiD gene*) or PdxK (PLK and PLK/HMPK-like products of *pdxK genes*) from the UniProt database. Other sequences with PLK activity annotated as PdxY were also incorporated, in addition to PdxK (PLK) from eukaryotic organisms.

The phylogenetic tree (Fig. 2, Supplementary Fig. S1) shows that PdxK proteins form two separate groups, where PLK/HMPPK-like enzymes (annotated mainly as PdxK and highlighted in purple) appear distant from the canonical PdxK proteins (shown in red). PLK/HMPPK-like enzymes (PdxK, purple) derived directly from ThiD, and only comprises sequences from gram-positive organisms, like the enzymes from *Staphylococcus aureus* [11] and *Bacillus subtilis* [5], which have been previously characterized with HMPK and PLK activity. On the other hand, all the ThiD enzymes (HMPPK) are clustered in one single group (highlighted in blue). Finally, the phylogeny shows that canonical PdxK (red) appear distant from the ThiD group (HMPPK), and are closer to the PLK encoded by the *pdxY* gene. Also, if the phylogeny is rooted in the eukaryotic PdxK (Supplementary Fig. S1), it is evident
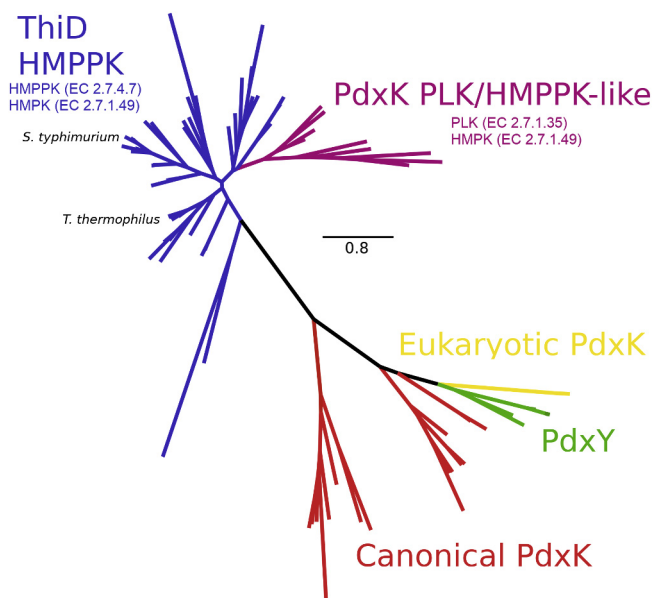
that canonical PdxK and ThiD diverged early. Overall, the topology of the branches within each group correlates well with their taxonomic categorization (Supplementary Fig. S1), which strongly suggests that the divergence between these enzymes occurred early during the bacterial evolutionary history.

3.2. HMPPKs from the order enterobacteriales and thermales can perform double phosphorylation of HMP

Purified *StHMPPK* was highly unstable at room temperature, with a strong trend to aggregate formation. After testing several conditions, we found that in the presence of 25 mM Tris-HCl pH 8.0 and 100 mM arginine the protein remains stable for hours. The addition of 20% glycerol maintains the protein stable for months at −80 °C. For purified *TtHMPPK*, optimal storage conditions included 25 mM Tris-HCl pH 8.0 and 300 mM NaCl.

To assess the ability of the *StHMPPK* and *TtHMPPK* enzymes to carry out the double phosphorylation of HMP, we performed stoichiometric analysis of the product ADP and the HMP substrate by employing a coupled assay with pyruvate kinase/lactate dehydrogenase and phosphoenolpyruvate that links the production of ADP to the consumption of NADH (Fig. 3A). In conditions where HMP is the limiting substrate, the phosphorylation of one molecule of ADP is coupled to the oxidation of one NADH molecule, and the NADH/ADP ratio should be 1:1. However, if HMP is phosphorylated twice, the oxidation of two NADH molecules is expected for each HMP consumed. ADP titration curves for both enzymes show a ratio [ADP/HMP] of 1.93 ± 0.30 and 1.73 ± 0.01 for *StHMPPK* and *TtHMPPK*, respectively (Fig. 3A). These results show that under equilibrium reaction conditions, two ADP molecules are generated per HMP consumed for both enzymes, suggesting the ability of these enzymes to perform two consecutive HMP phosphorylations.

To further assess the identity of the phosphorylated products, an anionic exchange HPLC was performed. Since changes are expected only in the phosphorylation degree of the HMP molecule, but not in the methylpyridine moiety, significant differences in the product retention times (HMP-P and HMP-PP) should be observed. Fig. 3B shows the chromatograms of the *StHMPPK* reaction products at different incubation times. A time-dependent disappearance of the first peak, corresponding to HMP, is observed. Also, a transient appearance of a second peak, which disappears when the reaction tends to equilibrium, was detected, and it could correspond to the HMP-P product. Finally, a sustained appearance of a third peak, that could be identified as HMP-PP, based on the number of its negative charges, was also detected. When the area under each peak is plotted as a function of time (Fig. 3C), a classical progress curve shape is observed for the appearance of HMP-PP, the disappearance of HMP, and the transient emergence of HMP-P. These results strongly support that the reaction stoichiometry determined for these enzymes is due to their ability to catalyze the double phosphorylation of HMP.

3.3. Substrate specificity

Previous characterizations of the HMPPK enzymes from *E. coli* [8], *S. aureus* [7], and *B. subtilis* [5] have shown that these enzymes are highly specific for HMP. This situation differs from what was reported for the PLK/HMPPK-like closely related homologs which are catalytically promiscuous, being able to phosphorylate HMP as well as different forms of vitamin B$_6$, like pyridoxal (PL), pyridoxine (PN) and pyridoxamine (PM) [11].

With the aim to evaluate if the substrate specificity reported for orthologous proteins is a conserved trait in the HMPPK from *S. typhimurium* and *T. thermophilus*, we assayed their activity using PL, PN, and PM as substrates (Fig. 3D). No significant ADP production was observed, in agreement with experiments previously reported for other HMPPKs, highlighting the fact that these enzymes are not promiscuous

Fig. 2. Schematic unrooted phylogenetic tree of ThiD and PdxK proteins. Branches were colored as follows: blue, ThiD (HMPPK); purple, PdxK (PLK/ HMPPK-like group); red, PdxK (canonical group); green, PdxY; yellow, eukaryotic PdxK. Enzymatic activities of interest are indicated with their respective EC number and experimentally characterized proteins in this work are depicted in the tree. (For interpretation of the references to color in this figure legend, the reader is referred to the Web version of this article.)
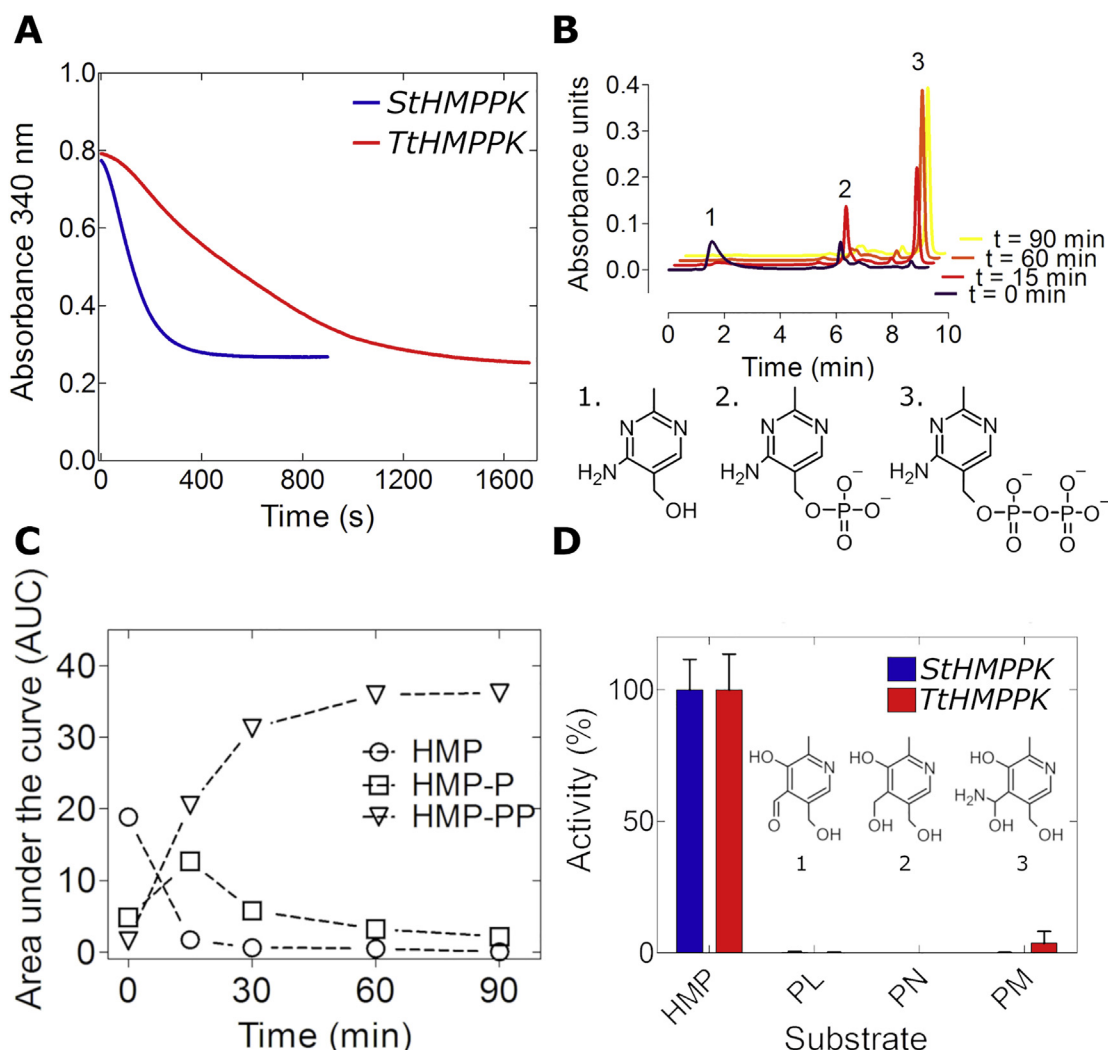
Fig. 3. Assessment of the capability of *StHMPPK* and *TtHMPPK* to perform double phosphorylation on HMP.
A) Representative titration curves of ADP production following the change of NADH absorbance for *StHMPPK* (blue) and *TtHMPPK* (red) in the presence of 50 μM HMP, 1 mM ATP, 6 mM MgCl$_2$ and 0.5 μM or 10 μM of *StHMPPK* and *TtHMPPK*, respectively. The [ADP/HMP] ratio was 1.93 ± 0.30 and 1.73 ± 0.01 for *StHMPPK* and *TtHMPPK*, respectively B) Chromatographic separation of the reaction products after different incubation times. The compounds were labeled as: 1 (HMP), 2 (HMP-P) and 3 (HMP-PP). C) Time courses of production and disappearance of HMP, HMP-P and HMP-PP were quantified as the area under the peak of the chromatograms shown in B. D) Relative activity of *StHMPPK* (blue bars) and *TtHMPPK* (red bars) in the presence of 100 μM of HMP, pyridoxal (PL), pyridoxine (PN), or pyridoxamine (PM). Results were normalized against the activity measured in the presence of HMP 300 μM ATP, 5 mM MgCl$_2$. The error bars correspond to the standard deviation of three replicates. All kinetic assays were performed in 50 mM HEPES pH 7.0 at 37 °C. (For interpretation of the references to color in this figure legend, the reader is referred to the Web version of this article.)

and that they only participate in the thiamine biosynthesis pathway.

3.4. Kinetic characterization

A more detailed kinetic analysis for *StHMPPK* and *TtHMPPK* was performed by measuring saturation curves for HMP at different MgATP concentrations. For *StHMPPK*, HMP saturation curves show a hyperbolic behavior (Fig. 4A). By fitting a Michaelis-Menten model to the data, changes in the apparent K$_M$ and V$_{max}$ values as a function of the MgATP concentration were obtained (Supplementary Table S1). From these results, information regarding the kinetic mechanism can be obtained.

For an ordered sequential mechanism, an equation for the change of the apparent K$_M$ for one substrate as a function of the co-substrate has been reported [21], which describes a hyperbole that intersects the Y-axis at a non-zero value (equation (3)). Analysis of the K$_M$ for HMP as a function of the MgATP concentration shows that indeed this is the behavior observed (Fig. 4B). In contrast, for a ping pong mechanism a

hyperbole intersecting the origin should be observed. So, this result strongly suggests that *StHMPPK* has a substrate-binding mechanism that involves a ternary complex formation, like the one described for other kinases from the ribokinase superfamily [20], discarding the ping-pong mechanism displayed by other phosphotransferases [34]. Thus, assuming an ordered sequential mechanism, the true K$_M$ values obtained for HMP and MgATP were 17 ± 1 μM and 0.74 ± 17 mM, respectively. On the other hand, the variation of the apparent V$_{max}$ as a function of the MgATP concentration (Fig. 4C), does not show a hyperbolic behavior. Instead, fitting the Hill equation to the data gives an *h* coefficient less than 1 (0.42 ± 0.02), which can be interpreted as strong negative cooperativity for MgATP or that more than one process is co-occurring during the reaction course. When the MgATP saturation curves were performed at high HMP concentrations (220 μM, insert Fig. 4D) fitting the Hill equation to the data gives an *h* coefficient of 0.40 (Fig. 4D). Otherwise, MgATP saturation curves at low concentration of HMP (4 μM), can be clearly adjusted to a hyperbolic behavior (insert Fig. 4D), showing that the cooperativity of the curves depends
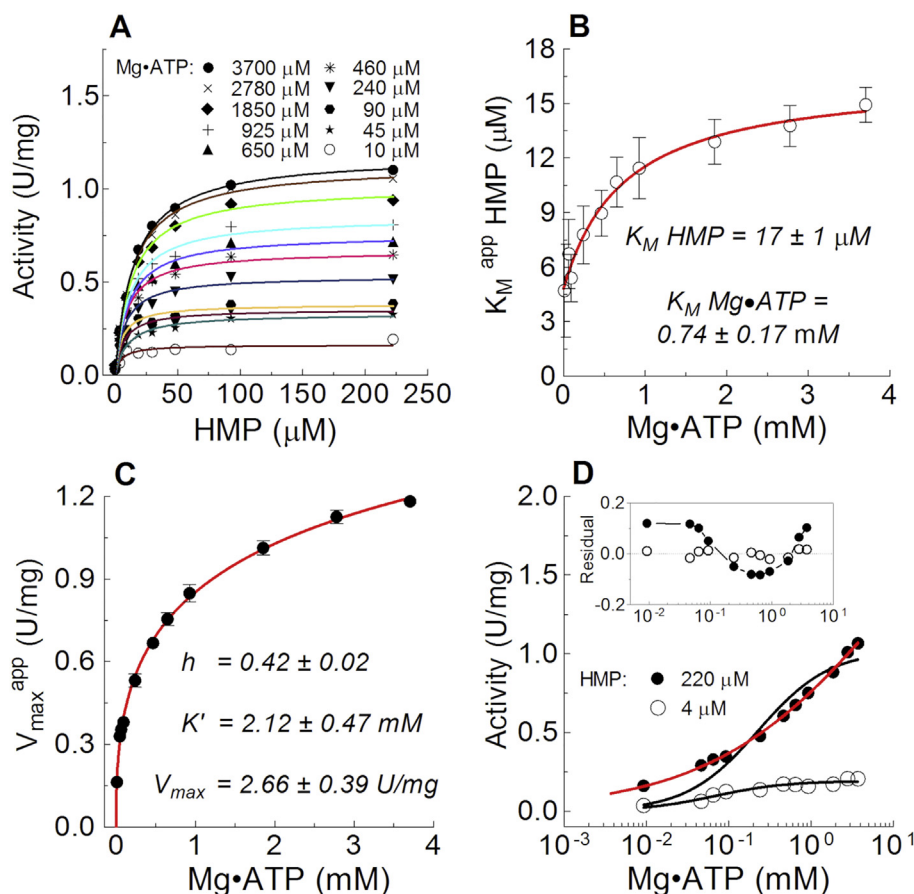
Fig. 4. Kinetic characterization of *StHMPPK*.
A) HMP saturation curves at several MgATP concentrations. A Michaelis-Menten equation was fitted to the data and apparent K_M and V_{max} were obtained. B) Variation of apparent K_M as a function of the ATP concentration. The best fit was a hyperbolic function with a non-zero value for Y-axis intersection (4.8 ± 0.4 mM) and giving K_M value of 17 ± 1 μM for HMP and 0.74 ± 0.17 mM for MgATP. C) Variation of apparent V_{max} as a function of MgATP concentration. Empirically the best fitting was to the Hill equation with an *h* index of 0.42 ± 0.02, a K′ of 2.12 ± 0.47 and a V_{max} extrapolated at infinite MgATP concentration of 2.66 ± 0.39 U/mg. D) MgATP saturations curves at high (220 μM) and low (4 μM) HMP concentrations. At high HMP concentrations (black circles) the MgATP saturation curve does not follow the Michaelis-Menten equation (black line), showing the best fit to the Hill equation (red line) with an *h* index of 0.40 ± 0.01. At low HMP concentration (white circles), the best fit is the Michaelis-Menten model. Insert: residual plot for fitting of the Michaelis-Menten model to the MgATP saturation curves. All assays were carried out at 25 °C with 25 mM HEPES pH 8.0, 5 mM in excess of $MgCl_2$ over the ATP concentration and 125 mM KCl. (For interpretation of the references to color in this figure legend, the reader is referred to the Web version of this article.)

on the HMP concentration.

Unfortunately, since for *TtHMPPK* the apparent K_M for HMP is less than 5 μM at all the MgATP concentrations tested (Supplementary Fig. S2), the saturation curves and the corresponding fittings present high statistical errors (Supplementary Table S2). Despite that, and considering the variation of V_{max} at different MgATP concentrations, the fit to the Hill equation also gives an *h* index less than 1, following the same trend observed with *StHMPPK*. Also, it is important to note that the K_M for HMP and MgATP (10 and 700 μM, respectively) were determined at 25 °C, far from the ecological niche temperature of *T. thermophilus* (65 °C).

3.5. Stability and structural differences between StHMPPK and TtHMPPK

The thermal stability of *StHMPPK* and *TtHMPPK* was assessed by determining the melting temperature (Tm) through circular dichroism at different temperature ramps (Fig. 5, Supplementary Table S3). The average Tm observerd for *TtHMPPK* was 83.1 °C, meanwhile for *StHMPPK* was 50.1 °C. In all the ramps tested, the *TtHMPPK* enzyme shows a difference in the Tm value of 30 °C or higher than the one for *StHMPPK*, confirming its high thermal stability.

To seek for determinants of thermal stability, we used the crystal structures for *StHMPPK* and *TtHMPPK* in the Apo form, available in the PDB (PDB 1JXH and 1UB0, respectively), to perform MDS of each system to get insights regarding their conformational dynamics. Analysis of the RMSD of both systems (insert graph, Fig. 6A), shows that for *StHMPPK* values are around 1 Å higher than for *TtHMPPK*. To search for differences in local flexibility, we calculated the RMSF per residue from the last 40 ns of the trajectories for both systems. Fig. 6A shows the average RMSF values derived from two replicas. Both proteins show a similar profile, where the regions exhibiting higher flexibility are conserved. Nevertheless, a significant difference in the magnitude of
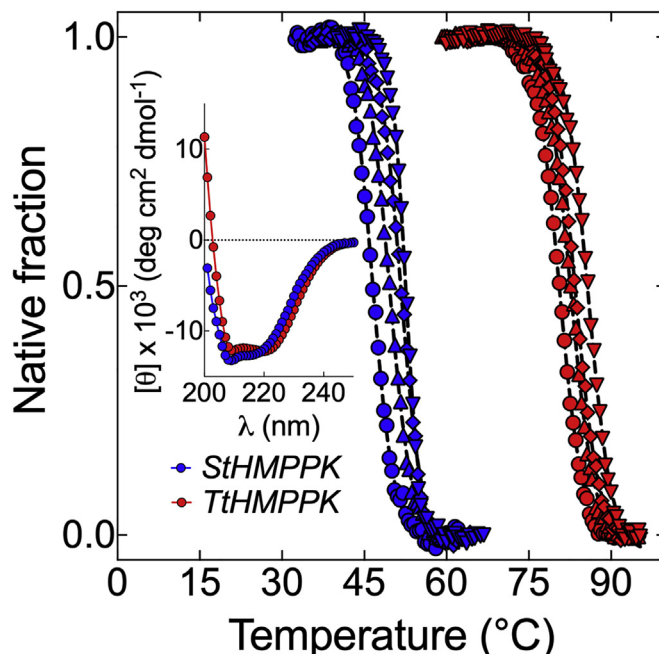

Fig. 5. Thermal stability of *StHMPPK* and *TtHMPPK*.
StHMPPK (blue) and *TtHMPPK* (red) assayed through CD with different temperature gradients, 0.5 (circle), 1.0 (up triangle), 2.0 (rhombus) and 3.0 (down triangle) °C/min. The insert shows the native CD spectra at 25 °C for *StHMPPK* (blue) and *TtHMPPK* (red). (For interpretation of the references to color in this figure legend, the reader is referred to the Web version of this article.)
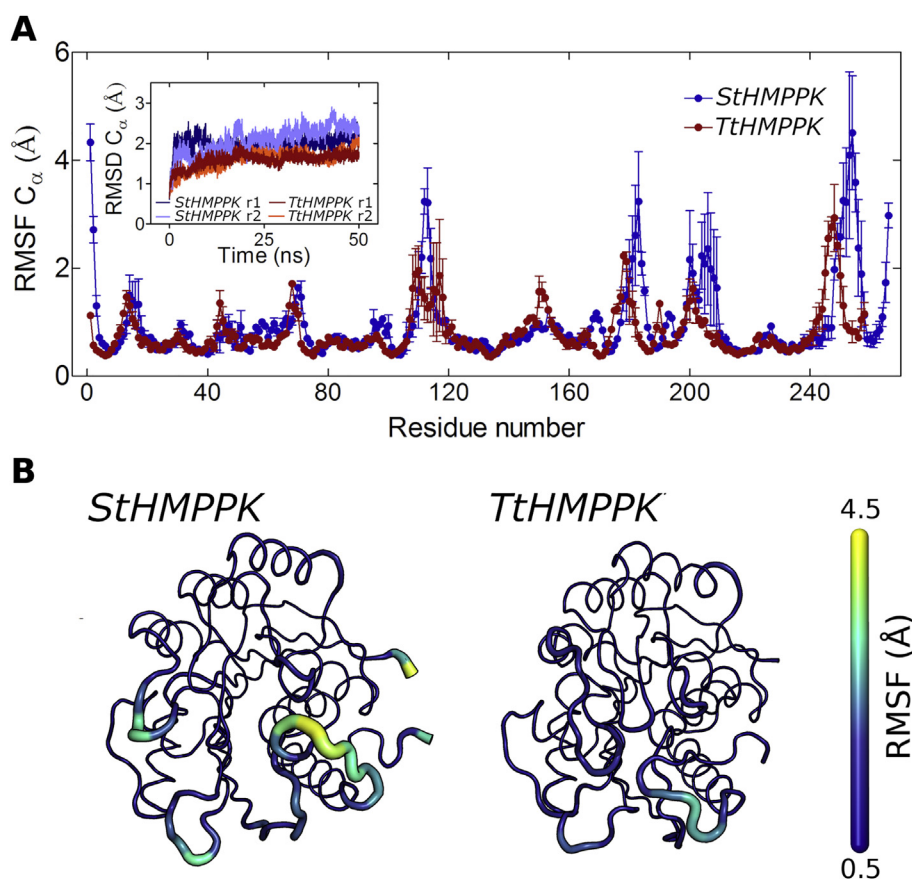
A

B

Fig. 6. **Conformational flexibility of *StHMPPK* and *TtHMPPK* assessed by molecular dynamics simulation.** A) RMSF variation per residue for *StHMPPK* (blue) and *TtHMPPK* (red). The inset shows the RMSD variation of the Cα during the trajectories for *StHMPPK* (blue and light blue for each replica) and *TtHMPPK* (red and orange for each replica). B) Differences in conformational flexibility between *StHMPPK* and *TtHMPPK* mapped on their respective structures. (For interpretation of the references to color in this figure legend, the reader is referred to the Web version of this article.)

this parameter is observed, indicating that structure fluctuations in *StHMPPK* are notoriously higher than those of *TtHMPPK*. Mapping the RMSF values on the respective protein structure shows that regions with higher flexibility are located nearby the active site of the enzymes as well as in the N- and C-terminal regions.(Fig. 6B).

To explore the structural determinants that could explain the striking differences in the conformational dynamics between *StHMPPK* and *TtHMPPK*, we analyzed some of the structural hallmarks commonly related to enhanced thermal stability, such as electrostatic interactions (i.e., hydrogen bonds and salt-bridges) [35–37] and hydrophobic effects [36,38,39]. First, we investigated the role of salt bridges (SB) and hydrogen bonds (HB) interactions using MDS trajectories obtained during simulations. SB were defined as interactions between oppositely charged residues within a distance no larger than 4.5 Å and persisting in at least 10% of the MDS time analyzed (Table 1). A total of 18 SB pairs were found in *StHMPPK* while for *TtHMPPK* 25 SB pairs could be recognized. Interestingly, a great number of the SB found in *TtHMPPK* are rather short-lived. These charged residues establish interactions with different partners and, therefore, create a more intricate

interaction network than its mesostable counterpart (Fig. 7A). Regarding the HB interactions, it is worth noticing that the total number does not correlate with differences in the thermal stability of these proteins, since during the molecular dynamics simulations, *TtHMPPK* showed a smaller number of HB than *StHMPPK* (Table 1). These results show that the number of SB, but not the number of HB, could directly contribute to the stabilization of the more thermostable protein architecture in these enzymes.

To asses if there were any significant differences in the hydrophobic cores, we analyzed the amino acid composition for both proteins. First, we chose representative structures from the MDS through cluster analysis, using the density-based scan algorithm implemented in cpptraj from Ambertools14 [24]. Residues were categorized as exposed to the surface or buried within the core depending on their exposed molecular surface area. Those with an exposed molecular surface > 5 Å^2 were considered to be exposed, otherwise they were considered as part of the protein core. The hydrophobic core of *TtHMPPK* has a higher content of apolar residues (Fig. 7B), mainly given by an increment of alanine and a slight reduction in polar residues (Supplementary Fig. S3). To analyze whether these changes have an impact on the number of hydrophobic interactions, we quantified the interatomic native contacts mediated by these residues in each protein. The results are shown as distribution histograms of the number of hydrophobic interatomic contacts per simulation frame (Fig. 7C). *StHMPPK* has an overall lower amount of interactions with a broader distribution curve than *TtHMPPK*, meaning that there is a remarkable difference in the hydrophobic packing of the mesostable and the thermostable protein.

Overall, the MDS results showed that *StHMPPK* and *TtHMPPK* have striking differences in their conformational flexibility that can be linked to their differences in the electrostatic interaction network, given mainly by the SB network and the hydrophobic packing of the structure.

Table 1
The total number of intramolecular interactions found during at least 10% of the simulation time in *StHMPPK* and *TtHMPPK*.

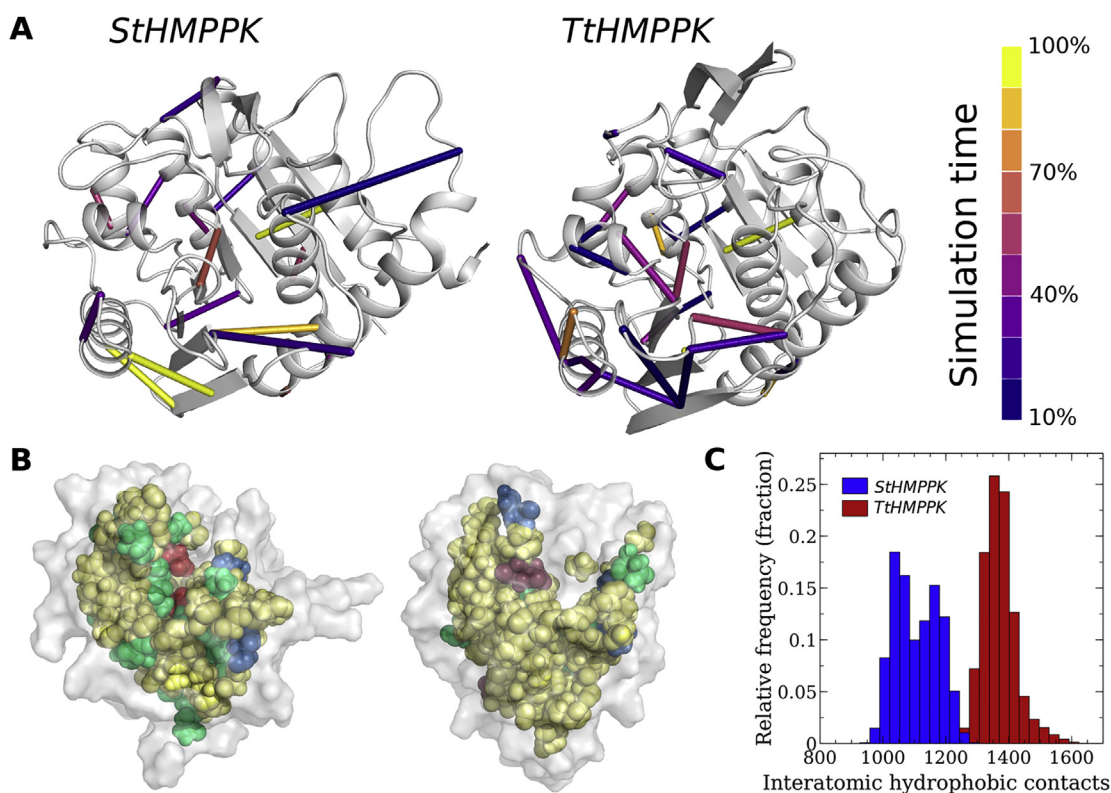| Type of Interaction	Protein	
	StHMPPK	*TtHMPPK*
Salt bridges	18	25
Inter-atomic native contacts between hydrophobic residues	1624	1846
Hydrophobic residues pairs forming native contacts	251	287
Hydrogen bonds between backbone atoms	194	186
Hydrogen bonds between side chains	99	69

Fig. 7. Quantification of electrostatic and hydrophobic interactions in *StHMPPK* and *TtHMPPK*.
A) Salt bridge (SB) interactions in *StHMPPK* and *TtHMPPK*. SB are shown as lines joining the Cα of the interacting residues and colored according to their permanence during the simulation time analyzed. B) Differences in the amino acid composition at the core of *StHMPPK* and *TtHMPPK* (shown as van der Waals spheres). Apolar residues are shown in yellow, non-charged polar residues are shown in green, acidic residues are shown in red and basic residues are shown in blue. C) Interatomic hydrophobic contacts in the structure of *StHMPPK* (blue), and *TtHMPPK* (red) identified in each simulation frame. (For interpretation of the references to color in this figure legend, the reader is referred to the Web version of this article.)

4. Discussion

Enzymes with HMP kinase activity constitute a heterogeneous group, where multiple proteins participating in different pathways can be found, generating miss annotation of their function. Our results from phylogenetic analysis shed light on the evolutionary history of these groups of enzymes. These results agree with what was proposed by Nodwell et al., and Newman et al. [10,11], that the enzymes referred as PLK/HMPPK-like constitute a distinct group from the canonical PLK and are closely related to the HMPP kinases encoded by the *thiD* gene. Since the gene annotation for PLK/HMPPK-like and canonical PLK remain the same (both referred to as products of a *pdx*K gene), our results help to establish that they are indeed different proteins and should be annotated distinctly to avoid further confusion.

The biochemical characterization of the HMPPK from *S. typhimurium* and *T. thermophilus* shows that they behave in a similar way regarding substrate specificity and catalytical properties to previously described HMPP kinases [5,7,8]. The high substrate specificity displayed by these enzymes also seems to be a conserved feature among them, which suggests that they only participate in the thiamine biosynthesis pathway. Stoichiometric analysis and time course experiments of product appearance indicate that both enzymes maintain the capability to catalyze two consecutive phosphorylations on HMP, even when they have been subjected to very different selective pressures, regarding the temperature of their niches, suggesting that this feature is conserved among all HMPPK and may correspond to a critical adaptation trait for thiamine biosynthesis.

A more in-depth look into the results, obtained from initial rate steady-state kinetics, also could give evidence for the two consecutive phosphorylation reactions catalyzed by these enzymes. If we analyze the deviation from the hyperbolic behavior of MgATP saturation curves at high HMP concentration obtained for *StHMPPK*, we found that these results are better modelled assuming strong negative cooperativity. However, at low HMP concentrations a better fit was obtained with a Michaelian model. An explanation for this phenomenon would rely on the product detection system used to follow the reaction; since ADP is the product measured in the coupled assay it must be considered that it is generated in both phosphorylation reactions. At high HMP concentrations, the availability of HMP-P required for the second reaction is increased, and thus, there are two independent ATP consuming reactions that contribute to the overall ADP production, which would explain the cooperative behavior. Conversely, when the HMP concentration is low, the second phosphorylation reaction (HMP-P phosphorylation) does not contribute significantly to the ADP production, regardless of the ATP concentration, so a hyperbolic behavior is observed. In addition, the negative cooperativity could be explained if the rate of the second phosphorylation is much slower than the first, which is consistent with reports from other HMPPK where the rate of the second phosphorylation is up to 80 fold slower [40].

From the steady-state kinetics, as well as information regarding the type of kinetic mechanism can also be obtained. Although the assays performed preclude to obtain the substrate-binding order, and also, product inhibition assays are difficult to perform in systems with intermediaries (such as HMP-P), the results strongly support that the reaction mechanism of *StHMPPK* proceeds through a ternary complex formation, discarding a ping pong mechanism and being an ordered sequential mechanism enough to fit the kinetic parameters, but not ruling out more complex mechanisms like random sequential. For the thermophilic enzyme *TtHMPPK*, an ordered sequential mechanism is also consistent with kinetic parameters, although such parameters are

valid only at 25 °C.

Given the remarkable differences in the ecological niches where *S. typhimurium* and *T. thermophilus* thrive and the high structural similarity of their HMPPK, they represent an excellent model to explore the structural basis of thermal stability in the vitamin kinases family. Regarding this, StHMPPK and *TtHMPPK* proteins showed thermal stability according to their ecological niches, displaying a difference of at least 30 °C in their Tm values. Considering that thermal stability has been established as a property deeply tied to conformational flexibility [41], we explored the underlying structural and dynamical differences between both proteins through MDS. Our results agree with the notion that, at short time scales (below μs), thermally stable proteins have a more rigid backbone than proteins from mesophilic organisms. These results are in good agreement with the idea of a trade-off between activity and stability, suggesting that the increased stiffness of the active site of *TtHMPPK* is needed to maintain protein stability [42]. Our analyses revealed that this feature could be mainly attributed to two structural features: a higher amount of electrostatic interactions and the hydrophobic packing. Numerous previous reports have pointed out that salt bridges play a significant role in the thermal stability of a protein, since the increasing number of interactions imply a higher enthalpic contribution to the native state [35–37]. Also, the contribution of the hydrophobic effect to protein stability has been extensively reviewed in the literature [36,38,39]. The presence of a bulkier apolar core in *TtHMPPK* might increase the entropic cost of its exposure to the solvent upon denaturation, thus making the unfolded state less favorable. Moreover, our results show that *TtHMPPK* has a sharper distribution of interatomic hydrophobic contacts along the MDS trajectories compared to StHMPPK, which has a broader distribution. This further supports the idea that a thermostable protein has restricted motions, due to the narrower space of conformations that can explore, whereas a mesostable protein can explore conformations with small and large number of hydrophobic interatomic contacts.

An increased number of hydrogen bonds has also been related to enhanced thermal stability [36]; however, *TtHMPPK* displays fewer hydrogen bonds than StHMPPK. This result supports the fact that the structural adaptations by which a protein becomes more thermostable than its mesophilic homologs strongly depend on the particular fold under study as well as on its particular evolutionary history [43]. Therefore, in the case of these two HMPPK enzymes analyzed in this work, hydrophobic packing and salt bridges would be the structural determinants of thermal stability. Nonetheless, further studies with other members of the vitamin kinase family should be carried out to determine the generality of this adaptation mechanisms.

5. Conclusions

Phylogenetic analysis showed that PLK/HMPPK-like and canonical PLK enzymes, both annotated as *pdxK*, have a different evolutionary history and must be annotated distinctly. Characterization of the *S. typhimurium* (StHMPPK) and *T. termophillus* (*TtHMPPK*) enzymes indicate that both can perform double phosphorylation on HMP, being specific for this substrate and thus only participate in the thiamine biosynthesis pathway. Besides, kinetic analyzes are consistent with the formation of a ternary complex during catalysis, which can be modelled through an ordered sequential mechanism. Molecular dynamics simulation studies to establish the structural traits for the differential thermal stability of these two enzymes show striking differences in their conformational flexibility, mainly near the active site regions. These variations can be associated with their hydrophobic packings and electrostatic interaction networks, given principally by the salt bridges networks, but not by the number of hydrogen bonds present.

Author contributions

PAC, JB, VG and VCF devised the project. PAC perform the

phylogenetic analysis. GA and PAC carried out and analyzed the kinetic experiments related to double phosphorylation, substrate specificity and thermostability. GV designed and performed the kinetic experiments. GV, VG and VCF analyzed the data for the kinetic mechanism. PAC, RR and JAM perform and analyzed the molecular dynamic simulations and PAC, VG, JB and VCF wrote the paper.

Declaration of competing interest

The authors declare no conflict of interest.

Acknowledgments

Appendix A. Supplementary data

Supplementary data to this article can be found online at https://doi.org/10.1016/j.abb.2020.108389.

References

[1] C.T. Jurgenson, T.P. Begley, S.E. Ealick, The structural and biochemical foundations of thiamin biosynthesis, Annu. Rev. Biochem. 78 (2009) 569–603.

[2] Q. Du, H. Wang, J. Xie, Thiamin (Vitamin B1) Biosynthesis and regulation: a rich source of antimicrobial drug targets? Int. J. Biol. Sci. 7 (2011) 41–52.

[3] N. Imamura, H. Nakayama, thiD locus of *Escherichia coli*, Experientia 37 (1981) 1265–1266.

[4] T. Mizote, H. Nakayama, Purification and properties of hydroxymethylpyrimidine kinase from Escherichia coli, BBA - Gen. Subj. 991 (1989) 109–113, https://doi.org/10.1016/0304-4165(89)90035-4.

[5] J.-H. Park, K. Burns, C. Kinsland, T.P. Begley, Characterization of two kinases involved in thiamine pyrophosphate and pyridoxal phosphate biosynthesis in B*acillus subtilis*: 4-Amino-5-Hydroxymethyl-2-Methylpyrimidine kinase and pyridoxal kinase, J. Bacteriol. 186 (2004) 1571–1573, https://doi.org/10.1128/JB.186.5.1571-1573.2004.

[6] G. Cheng, E.M. Bennett, T.P. Begley, S.E. Ealick, Crystal structure of 4-amino-5-hydroxymethyl-2-methylpyrimidine phosphate kinase from *Salmonella typhimurium* at 2.3 A resolution, Structure 10 (2002) 225–235.

[7] I.B. Müller, B. Bergmann, M.R. Groves, I. Couto, L. Amaral, T.P. Begley, R.D. Walter, C. Wrenger, The vitamin B1 metabolism of *Staphylococcus aureus* is controlled at enzymatic and transcriptional levels, PloS One 4 (2009) e7656.

[8] J.J. Reddick, C. Kinsland, R. Nicewonger, T. Christian, D.M. Downs, M.E. Winkler, T.P. Begley, Overexpression, purification and characterization of two pyrimidine kinases involved in the biosynthesis of thiamin: 4-amino-5-hydroxymethyl-2-methylpyrimidine kinase and 4-amino-5-hydroxymethyl-2-methylpyrimidine phosphate kinase, Tetrahedron 54 (1998) 15983–15991.

[9] M.-H. Li, F. Kwok, W.-R. Chang, C.-K. Lau, J.-P. Zhang, S.C.L. Lo, T. Jiang, D.-C. Liang, Crystal structure of brain pyridoxal kinase, a novel member of the ribokinase superfamily, J. Biol. Chem. 277 (2002) 46385–46390.

[10] J.A. Newman, S.K. Das, S.E. Sedelnikova, D.W. Rice, The crystal structure of an ADP complex of *Bacillus subtilis* pyridoxal kinase provides evidence for the parallel emergence of enzyme activity during evolution, J. Mol. Biol. 363 (2006) 520–530.

[11] M.B. Nodwell, M.F. Koch, F. Alte, S. Schneider, S.A. Sieber, A subfamily of bacterial ribokinases utilizes a hemithioacetal for pyridoxal phosphate salvage, J. Am. Chem. Soc. 136 (2014) 4992–4999.

[12] M.K. Safo, F.N. Musayev, M.L. di Salvo, S. Hunt, J.-B. Claude, V. Schirch, Crystal structure of pyridoxal kinase from the *Escherichia coli* pdxK gene: implications for the classification of pyridoxal kinases, J. Bacteriol. 188 (2006) 4542–4552.

[13] T. Mizote, M. Tsuda, D.D.S. Smith, H. Nakayama, T. Nakazawa, Cloning and characterization of the thiD/J gene of *Escherichia coli* encoding a thiamin-synthesizing bifunctional enzyme, hydroxymethyIpyrimidine kinase/phosphomethylpyrimidine kinase, Microbiology 145 (1999) 495–501.

[14] M.B. Nodwell, H. Menz, S.F. Kirsch, S.A. Sieber, Rugulactone and its analogues exert antibacterial effects through multiple mechanisms including inhibition of thiamine biosynthesis, Chembiochem (2012), https://doi.org/10.1002/cbic.201200265.

[15] V. Castro-Fernandez, F. Bravo-Moraga, C.A. Ramirez-Sarmiento, V. Guixe, Emergence of pyridoxal phosphorylation through a promiscuous ancestor during the evolution of hydroxymethyl pyrimidine kinases, FEBS Lett. 588 (2014) 3068–3073.

[16] A. Bateman, UniProt: a worldwide hub of protein knowledge, Nucleic Acids Res. 47 (2019) D506–D515.

[17] J. Pei, B.H. Kim, N.V. Grishin, PROMALS3D: a tool for multiple protein sequence and structure alignments, Nucleic Acids Res. 36 (2008) 2295–2300.

[18] F. Abascal, R. Zardoya, D. Posada, ProtTest: selection of best-fit models of protein

evolution, Bioinformatics 21 (2005) 2104–2105.

[19] S. Guindon, J.F. Dufayard, V. Lefort, M. Anisimova, W. Hordijk, O. Gascuel, New algorithms and methods to estimate maximum-likelihood phylogenies: assessing the performance of PhyML 3.0, Syst. Biol. 59 (2010) 307–321.

[20] A. Herrera-Morande, V. Castro-Fernández, F. Merino, C.A. Ramírez-Sarmiento, F.J. Fernández, M. Cristina Vega, V. Guixé, Protein topology determines substrate-binding mechanism in homologous enzymes, BBA - Gen. Subj. 1862 (2018) 2869–2878.

[21] W.W. Cleland, Enzyme kinetics: steady state, Encycl. Life Sci. John Wiley & Sons, Ltd, Chichester, UK, 2009, pp. 1–5, https://doi.org/10.1038/npg.els.0000719.

[22] M.H.M. Olsson, C.R. Søndergaard, M. Rostkowski, J.H. Jensen, PROPKA3: consistent treatment of internal and surface residues in empirical pKa predictions, J. Chem. Theor. Comput. 7 (2011) 525–537.

[23] W.L. Jorgensen, Quantum and statistical mechanical studies of liquids. 10. Transferable intermolecular potential functions for water, alcohols, and ethers. Application to liquid water, J. Am. Chem. Soc. 103 (1981) 335–340.

[24] D.A. Case, T.E. Cheatham, T. Darden, H. Gohlke, R. Luo, K.M. Merz, A. Onufriev, C. Simmerling, B. Wang, R.J. Woods, The Amber biomolecular simulation programs, J. Comput. Chem. 26 (2005) 1668–1688.

[25] V. Hornak, R. Abel, A. Okur, B. Strockbine, A. Roitberg, C. Simmerling, Comparison of multiple Amber force fields and development of improved protein backbone parameters, Proteins Struct. Funct. Bioinfo. 65 (2006) 712–725.

[26] H.J.C. Berendsen, J.P.M. Postma, W.F. van Gunsteren, J. Hermans, Interaction models for water in relation to protein hydration, in: B. Pullman (Ed.), Jerusalem Symp. Quantum Chem. Biochem. vol. 14, Springer, Dordrecht, 1981, pp. 331–342.

[27] H.J.C. Berendsen, J.P.M. Postma, W.F. van Gunsteren, A. DiNola, J.R. Haak, Molecular dynamics with coupling to an external bath, J. Chem. Phys. 81 (1984) 3684–3690.

[28] D.A. Case, V. Babin, J.T. Berryman, R.M. Betz, Q. Cai, D.S. Cerutti, T.E. Cheatham III, T.A. Darden, R.E. Duke, H. Gohlke, A.W. Goetz, S. Gusarov, N. Homeyer, P. Janowski, J. Kaus, I. Kolossváry, A. Kovalenko, T.S. Lee, S. LeGrand, T. Luchko, R. Luo, B. Madej, K.M. Merz, F. Paesani, D.R. Roe, A. Roitberg, C. Sagui, R. Salomen-Ferrer, G. Seabra, G.L. Simmerling, W. Smith, J. Swails, R.C. Walker, J. Wang, R.M. Wolf, X. Wu, P.A. Kollman, AMBER14, Univ. California, San Fr, 2014.

[29] J.-P. Ryckaert, G. Ciccotti, H.J.C. Berendsen, Numerical integration of the cartesian equations of motion of a system with constraints: molecular dynamics of n-alkanes, J. Comput. Phys. 23 (1977) 327–341.

[30] T. Darden, D. York, L. Pedersen, Particle mesh Ewald: an N log(N) method for Ewald sums in large systems, J. Chem. Phys. 98 (1993) 10089–10092.

[31] D.R. Roe, T.E. Cheatham, PTRAJ and CPPTRAJ: software for processing and analysis of molecular dynamics trajectory data, J. Chem. Theor. Comput. 9 (2013) 3084–3095.

[32] W. Humphrey, A. Dalke, K. Schulten, VMD: visual molecular dynamics, J. Mol. Graph. 14 (1996) 33–38.

[33] R. Rodriguez, G. Chinea, N. Lopez, T. Pons, G. Vriend, Homology modeling, model and software evaluation: three related resources, Bioinformatics 14 (1998) 523–528.

[34] H. Yu, X. Rao, K. Zhang, Nucleoside diphosphate kinase (Ndk): a pleiotropic effector manipulating bacterial virulence and adaptive responses, Microbiol. Res. 205 (2017) 125–134.

[35] S. Kumar, C.-J. Tsai, B. Ma, R. Nussinov, Contribution of salt bridges toward protein thermostability, J. Biomol. Struct. Dyn. 17 (2000) 79–85.

[36] F. Pucci, M. Rooman, Physical and molecular bases of protein thermal stability and cold adaptation, Curr. Opin. Struct. Biol. 42 (2017) 117–128.

[37] A.S. Thomas, A.H. Elcock, Molecular simulations suggest protein salt bridges are uniquely suited to life at high temperatures, J. Am. Chem. Soc. 126 (2004) 2208–2214.

[38] M.M. Gromiha, M.C. Pathak, K. Saraboji, E.A. Ortlund, E.A. Gaucher, Hydrophobic environment is a key factor for the stability of thermophilic proteins, Proteins Struct. Funct. Bioinfo. 81 (2013) 715–721.

[39] P.J. Haney, J.H. Badger, G.L. Buldak, C.I. Reich, C.R. Woese, G.J. Olsen, Thermal adaptation analyzed by comparison of protein sequences from mesophilic and extremely thermophilic *Methanococcus* species, Proc. Natl. Acad. Sci. U. S. A 96 (1999) 3578–3583.

[40] C. Wrenger, M.-L. Eschbach, I.B. Müller, N.P. Laun, T.P. Begley, R.D. Walter, Vitamin B1 de novo synthesis in the human malaria parasite *Plasmodium falciparum* depends on external provision of 4-amino-5-hydroxymethyl-2-methylpyrimidine, Biol. Chem. 387 (2006) 41–51.

[41] P.A. Fields, Review: protein function at thermal extremes: balancing stability and flexibility, Comp. Biochem. Physiol. Mol. Integr. Physiol. 129 (2001) 417–431.

[42] G. Feller, Protein stability and enzyme activity at extreme biological temperatures, J. Phys. Condens. Matter 22 (2010) 323101.

[43] G.A. Petsko, [34] Structural basis of thermostability in hyperthermophilic proteins, or "There's more than one way to skin a cat, Methods Enzymol. 2001, pp. 469–478.